TCABSE-J Research Article
ISSN: 2583- 2557, *Volume 1, Issue 8, pp19-24. 2024.*

In silico identification and QSAR analysis of small molecule inhibitors for glucose transporter 3, a potential drug target for pan cancer treatments

Shahid A. Laskar, Manikanta Sodasani and Ravikiran S. Yedidi*

Department of Intramural research core, The Center for Advanced-Applied Biological Sciences & Entrepreneurship (TCABS-E), Visakhapatnam 530003, A.P. India.

(*Correspondence to R.S.Y.: tcabse.india@gmail.com).

Keywords: Diabetes, glucose transporters, GLUT3, inhibitors, anti-cancer drugs, oncology therapeutics.

Transport of glucose into the human cells is facilitated by members of the glucose transporters such as GLUT1-14 of SLC2A gene family, out of which GLUT3 is an important glucose transporter for the cancer metastasis as it shows high expression rate in colorectal cancer, gastric cancer and various other cancers. In this study we screened around 509 ligands from the Zinc database and identified 2 ligands with the highest binding affinity against GLUT3. These compounds were further developed by QSAR analysis followed by molecular dynamic simulations. The QSAR improved the binding affinity of both ligands against GLUT3. Considering the frequency of overexpression of GLUT3 in pan cancer, these GLUT3 inhibitors may be very specific in controlling the glucose molecules entry into various cancer cells to metastasis, resulting in new therapeutic pathways in oncology.

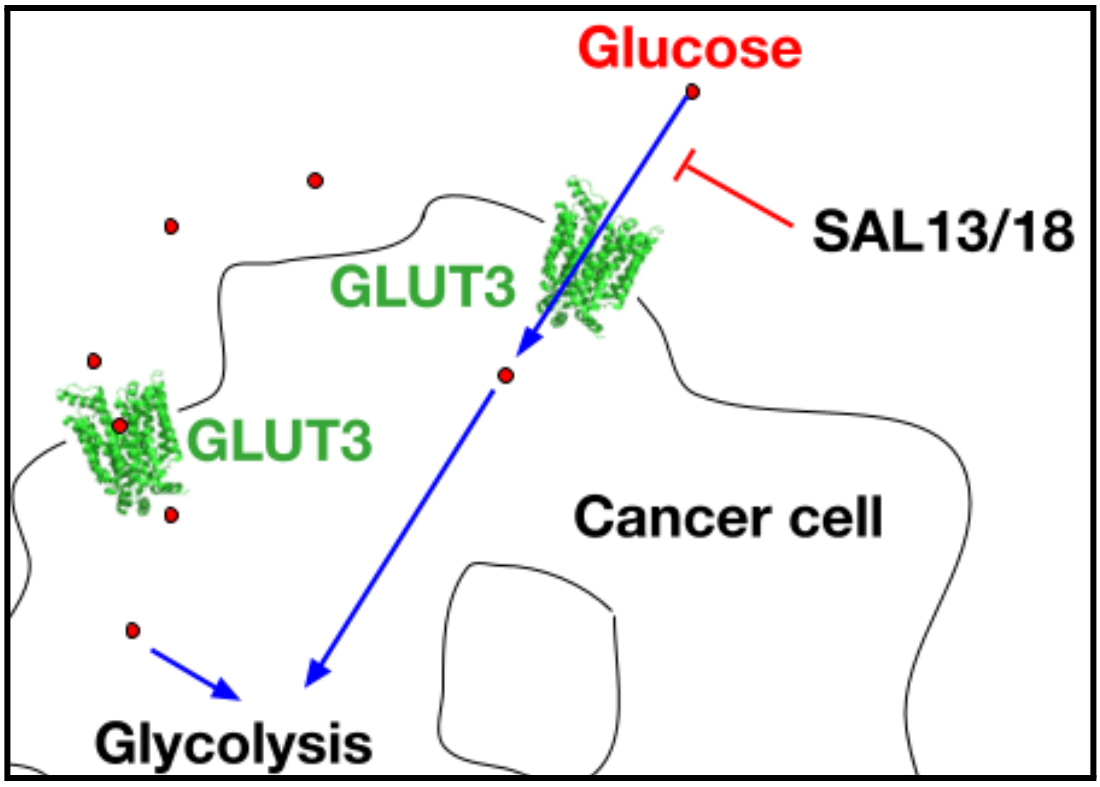

Citation: Laskar, S.A., Sodasani, M. and Yedidi, R.S. (2024). *In silico* identification and QSAR analysis of small molecule inhibitors for glucose transporter 3, a potential drug target for pan cancer treatments *TCABSE-J*, Vol. 1, Issue 8:19-24. Epub: Sep 30th, 2024.

TCABSE-J Research Article
ISSN: 2583- 2557, *Volume 1, Issue 8, pp19-24. 2024.*
TCABSE-J Interdisciplinary Sciences Journal

Glucose is the main energy source for the body as it provides the required energy to the cells and the tissues to perform optimally, in the brain, muscles and other essential tissues. Glucose is transported across the cell membranes and the proteins that facilitate glucose uptake are called Glucose Transporter Proteins (GLUTs) which are membrane bound proteins from the family SLC2A. About 14 GLUT proteins are expressed in the human body which can be classified into 3 classes based on their structural and sequence similarity. Each GLUT consists of about 500 amino acid residues [1]. Glycolysis is the process of breakdown of glucose into lactate. Under hypoxic conditions one molecule of glucose yields 36 to 38 molecules of ATP and under anaerobic conditions 2 ATP molecules. However, ATP will be generated in less quantities as it will produce lactate in the cytoplasm through lactate dehydrogenase (LDH). This phenomenon is known as the Warburg Effect. [2-4].

All cells need a source of energy to maintain homeostasis. However, cancer cells have additional energy requirements due to their constant growth and division. Tumor cells require large amounts of nutrients and energy to replicate [5]. These cancer cells mainly rely on glucose metabolism to grow and divide rapidly. Due to the anaerobic conditions, the ATP formation is less due to the Warburg effect [4]. As the demand of glucose increases most cancers show changes in the expression of GLUT. GLUT3 is upregulated in several cancers correlating with tumor aggressiveness in brain [6-8], lung [9-10], laryngeal [11], breast [12], gastric [13], liver [14] and colorectal cancers [15].

As glucose is hydrophilic in nature it cannot penetrate the plasma membrane of lipid bilayer. Human GLUTs belong to the Major facilitator superfamily (MFS). Glucose transport can take place across the cellular membrane which require specific carrier proteins called Glucose Transporters [1, 16]. Human GLUTs have 14 members of the sodium-independent glucose transporters, from GLUT1–GLUT14 which are encoded by the SLC2A1–SLC2A14 genes, respectively [17]. These glucose transporters contain 12 hydrophobic α-helical transmembrane (TM) domains which are linked with the hydrophilic loop between transmembrane (TM6) and transmembrane (TM7) of Glucose transporter protein [18]. GLUT proteins are characterized in a short intracellular N-terminal segment and a large C-terminal segment and also contain a single site for glycosylation on the exofacial end and in the large loop between TM1 and TM2 or between TM9 and TM10 [1].

Comparing all the sequences of all GLUTs, which apparently shows that the putative TM regions exhibit greater similarities, whereas the sequences within the loops and the C- and N-termini, shows more differences [19]. GLUT proteins are categorized into three classes in which Class I encodes with GLUT1 to GLUT4 and GLUT14, whereas Class II comprises GLUT5, GLUT7, GLUT9, and GLUT 11

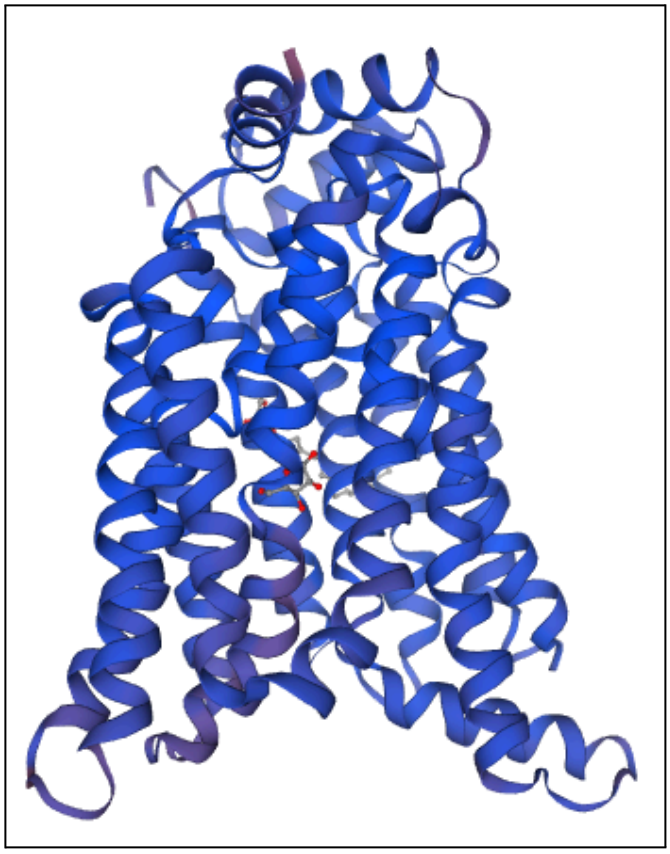

Figure 1. Homology model of human GLUT3.

and on the other hand Class III comprises GLUT6, GLUT8, GLUT10, GLUT12 and GLUT13 (HMIT) [19, 20] when analyses based on the phylogenetic analysis of sequence analysis. GLUT13 which is an H^+/myo-inositol symporter is an exception as all the GLUTs follow facilitated transport [21].

The proposed transport mechanisms for Major Facilitator Superfamily (MFS) proteins includes a variety of models, such as the alternate access mechanism and the fixed-site transporter model [22], in the alternate access mechanism, the substrate cavity shows a rhythmic pattern of exposure to the external environment (outward-facing or exo-facial conformation) and the internal environment (inward-facing or endo-facial conformation) of the cell [23]. On the other hand, the fixed-site transporter model proposes the simultaneous existence of exo- and endo-facial conformations [24, 25]. These foundational ideas, particularly highlighted in the context of the GLUT1 protein, have gained significant attention due to the validation provided by crystal structures of various human GLUTs (such as GLUT1, GLUT3, and GLUT5) and their counterparts, capturing both outward- and inward-facing conformations in exquisite detail [26-28]. Through these structural representations, the presence of substrate binding

TCABSE-J Research Article
ISSN: 2583- 2557, *Volume 1, Issue 8, pp19-24. 2024.*

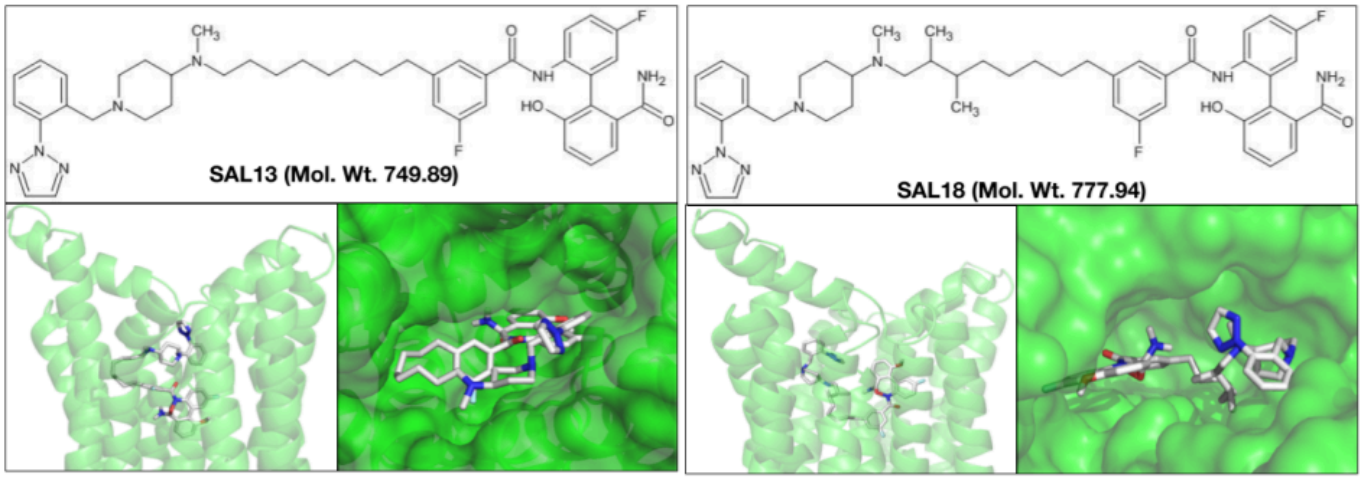

Figure 2. SAL3 and SAL18 structures and binding profiles.

sites are unveiled, showing them in either accessible (open state) or shielded (occluded state) configurations, shedding light on the intricate mechanisms governing protein transport in biological systems. These structures help in the homology structure modeling of GLUT isoforms for computational ligand screening, which allows for discovery and identification of specific ligands that interact with GLUT proteins [29-31].

In this study we used the GLUT3 as the drug target (receptor) and screened for hits (small molecules) from the Zinc database [32]. The hits were further optimized by *in silico* quantitative structure-activity relationship (QSAR) analysis to enhance their binding affinities.

Materials & Methods:

GLUT3 homology modeling: Amino acid sequence of the human GLUT3 protein was copy-pasted into the SWISS MODEL server (https://swissmodel.expasy.org) and a homology model was built with a sequence identity of 99.8%. Coordinates of the final model were downloaded and were used for virtual screening, docking and molecular dynamics simulations. The 3D model is shown in Figure 1.

Virtual screening from the Zinc database: The homology model of human GLUT3 was used as a receptor for docking and a virtual screen was performed using the ZINC database (https://zinc.docking.org/). Around 509 compounds that were closely related to the human GLUT1 were screened virtually to identify the hit molecules. SWISS Dock in combination with Chimera were used for docking the compounds from the ZINC database. Compounds were ranked based on their binding affinity values followed by their binding orientations in the binding pocket of the receptor, the human GLUT3.

QSAR analysis of hit molecules: The QSAR analysis of hit compounds from the ZINC database was performed using ChemSketch software from ACD Labs (Freeware) v2021.2.0 (www.acdlabs.com) for building the 2D and 3D versions of the small molecules. The 3D models were then docked into the binding pocket of the human GLUT3 receptor using AutoDock-Vina as described previously [33].

Molecular dynamics simulations: MD simulations of human GLUT3 homology model docked with either SAL13 or SAL18 were subjected to 15 ns of MD simulations each using Desmond (D. E. Shaw LLC, New York) as described previously [34]. Simulation interactions diagrams were prepared using the Maestro graphics user interface from Schrödinger (Schrödinger LLC, New York). Root mean square deviations (RMSD) and root mean square fluctuations (RMSF) of the protein C_α atoms were obtained from the simulation trajectories.

Results and Discussion:

Virtual screening identifies 2 hit molecules from the ZINC database: Virtual screening of 509 compounds yielded 2 hit compounds, ZINC299854414 (Mol. Wt.: 680) and ZINC49605358 (Mol. Wt.: 670) with binding affinity values -11.74 kcal/mol. and -11.24 kcal/mol., respectively. These binding affinity values were obtained from the docking outputs of SWISS DOCK. The same two compounds were then re-docked into the same receptor using AutoDock-Vina and it was found that the binding affinity values decreased slightly. The AutoDock-Vina docking scores against the same receptor for ZINC299854414 and ZINC49605358 were -8.5 kcal/mol. and -9.2 kcal/mol., respectively, with a difference of 3.24 - 1.34 kcal/mol.

TCABSE-J Research Article
ISSN: 2583- 2557, *Volume 1, Issue 8, pp19-24. 2024.*

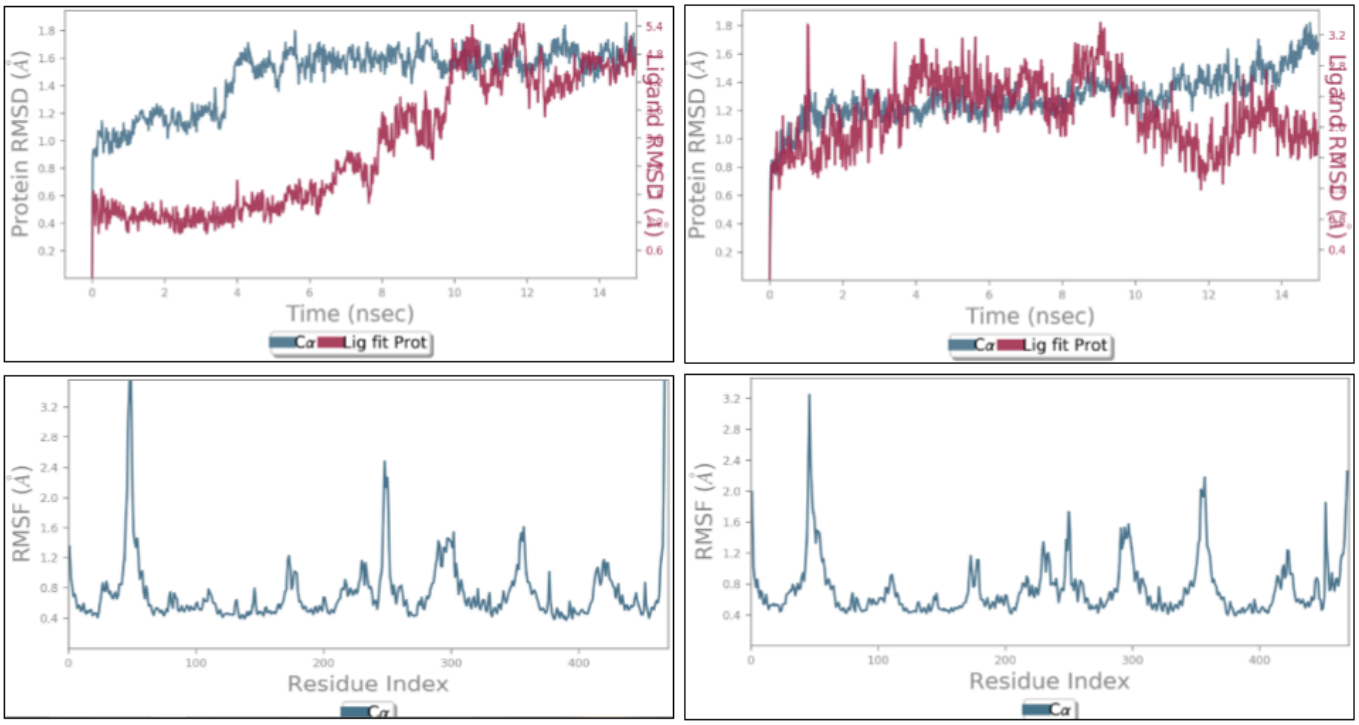

Figure 3. MD simulations of GLUT3-SAL13 (left)/SAL18 (right)

QSAR-optimization of binding affinities: One of the 2 hit compounds from the ZINC database was further modified by visualizing the compound in the binding pocket of the GLUT3 in PyMol. SWISS Bioisostere [35] was also used to find better QSAR modifications in addition to the manual modifications. After several rounds of QSAR and docking, the hit compound exhibited improved binding affinity. As shown in Figure 2, SAL13 and SAL18 (both QSAR-optimized from ZINC49605358) are the resultant molecules with binding affinity values of -11.5 kcal/mol. and -11.6 kcal/mol., respectively, against the human GLUT3 protein. These binding affinity values are based on the AutoDock-Vina scoring and are higher than the corresponding parent molecule's binding affinity (-9.2 kcal/mol.). These results suggest that both SAL13 and SAL18 are equipotent with respect to their binding affinities against the human GLUT3 protein.

Molecular dynamic simulations reveal differential backbone movements in GLUT3 with SAL13 and SAL18: MD simulations of GLUT3 docked with SAL13/SAL18 revealed that the overall RMSD and RMSF profiles of the protein C_α atoms are different. As shown in Figure 3 the overall RMSD of GLUT3 with SAL13 (top left panel) rose to 1.6 Å within the first 5 ns of the simulation while the overall RMSD of GLUT3 with SAL18 (top right panel) slowly rose to 1.6 Å in the last 5 ns of the simulation. These results suggest that the protein moved first in order to accommodate the movements of SAL13 while SAL18 pushed the protein to move potentially due to its additional methyl groups.

The RMSF of GLUT3 displayed differential profiles for SAL13 and SAL18. As seen in Figure 3, SAL13 bound GLUT3 (bottom left panel) has more RMSF within the first 100 amino acid residues followed by residues around 250. On the other hand SAL18 bound GLUT3 (bottom right panel) has comparatively less RMSF within the first 100 amino acid residues followed by additional RMSF around 350 while maintaining the RMSF at 250. Taken together, both SAL13 and SAL18 induce differential RMSF within the GLUT3 protein over 15 ns MD simulations.

Both SAL13 and SAL18 showed consistent contacts with GLUT3 over 15 ns MD simulations: Except for 2 additional methyl groups, SAL18 is structurally identical to SAL13. Both SAL13 and SAL18 showed persistent contacts with the GLUT3 throughout the 15 ns MD simulation. As shown in Figure 4 (left column) SAL13 primarily displayed more hydrophobic interactions (pale purple bars) along with hydrogen bonds (green bars) and water bridges (blue bars). SAL18 (Figure 4, right column) primarily exhibited more hydrogen bonds (green bars) along with hydrophobic interactions (pale purple bars) and water bridges (blue bars).

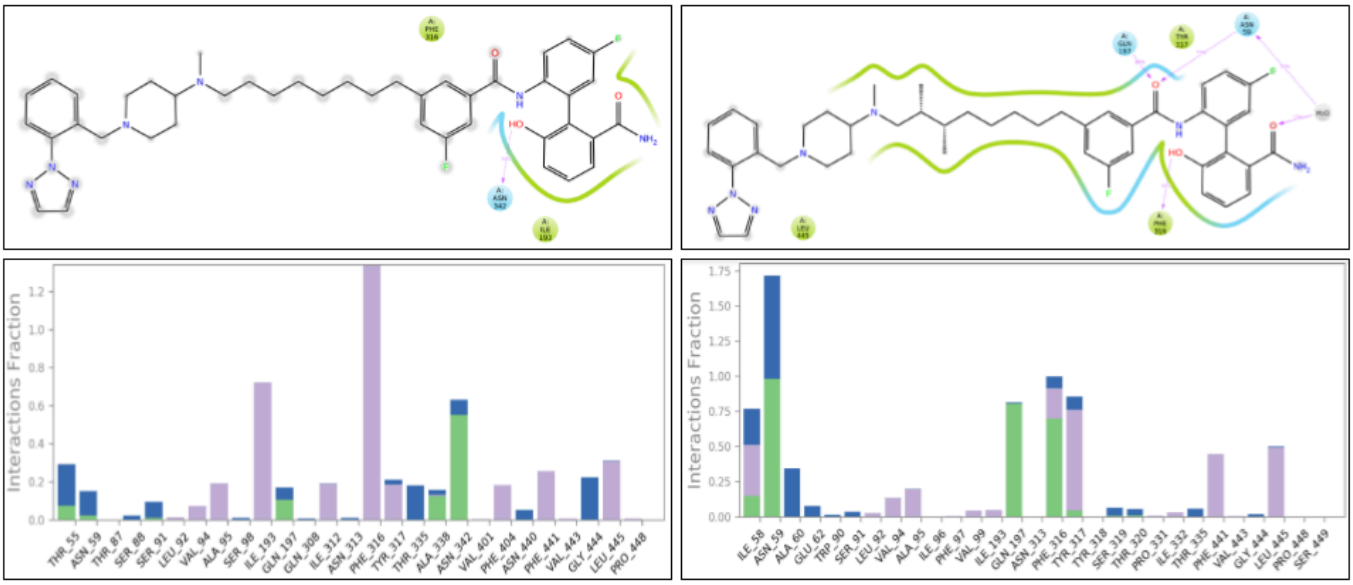

Figure 4. SAL13 (left) and SAL18 (right) binding profiles.

As seen in Figure 4, the additional methyl groups of SAL18 are involved in hydrophobic interactions (green highlighting line). These hydrophobic interactions lead to the formation of an additional contact with Leu445 in the triazole ring area for SAL18 suggesting that its binding profile is better than that of SAL13.

Conclusion and Future directions:

In the current study, we performed the QSAR-optimization of a hit molecule from the ZINC database screened against the human GLUT3 protein. Our *in silico* optimizations improved the binding affinity of the hit molecule. SAL18 has a better binding profile than SAL13 even though both exhibited similar binding affinity values against the human GLUT3 protein. In future, both SAL13 and SAL18 will be synthesized and evaluated in vitro to confirm the current findings.

Acknowledgements: We thank The Yedidi Institute of Discovery and Education, Toronto for scientific collaborations.

Conflict of interest: The authors declare no conflict of interest in this study.

Author contributions: S.A.L. performed virtual screening, docking, QSAR-optimization and structural analysis. M.S. supervised S.A.L. R.S.Y. performed MD simulations and trajectory analysis and is the principal investigator who designed the project, trained S.A.L. and M.S., secured required material for the project, provided the laboratory space and facilities needed. S.A.L. wrote the draft of the manuscript. R.S.Y. edited and finalized the manuscript.

References

1. Mueckler, M. & Thorens, B. The SLC2 (GLUT) family of membrane transporters. Mol. Aspects Med. 34, 121–138 (2013).
2. Lunt S.Y., Vander Heiden M.G. Aerobic glycolysis: Meeting the metabolic requirements of cell proliferation. *Annu. Rev. Cell Dev. Biol.* 2011;27:441–464. doi: 10.1146/annurev-cell bio-092910-154237.
3. Pavlova N.N., Thompson C.B. The emerging hallmarks of cancer metabolism. *Cell Metab.* 2016;23:27–47. doi: 10.1016/ j.cmet.2015.12.006.
4. Warburg O. The chemical constitution of respiratory ferment. *Science.* 1928;68:437–443. doi: 10.1126/science.68. 1767.437.
5. Liu, C.-L.; Hsu, Y.-C.; Lee, J.-J.; Chen, M.-J.; Lin, C.-H.; Huang, S.-Y.; Cheng, S.-P. Targeting the Pentose Phosphate Pathway Increases Reactive Oxygen Species and Induces Apoptosis in Thyroid Cancer Cells. *Mol. Cell. Endocrinol.* 2020, *499*, 110595.
6. Barron, C. C., Bilan, P. J., Tsakiridis, T. & Tsiani, E. Facilitative glucose transporters: Implications for cancer detection, prognosis and treatment. *Metab. Clin. Exp.* 65, 124–139 (2016).
7. Flavahan, W. A. *et al.* Brain tumor initiating cells adapt to restricted nutrition through preferential glucose uptake. *Nat. Neurosci.*16, 1373–1382 (2013).
8. Libby, C. J. *et al.* A role for GLUT3 in glioblastoma cell invasion that is not recapitulated by GLUT1. *Cell Adh. Migr.* 15, 101–115 (2021).
9. Younes, M., Brown, R. W., Stephenson, M., Gondo, M. & Cagle, P. T. Overexpression of Glut1 and Glut3 in stage I

nonsmall cell lung carcinoma is associated with poor survival. *Cancer* 80, 1046–1051 (1997).
10. Masin, M. *et al.* GLUT3 is induced during epithelial-mesenchymal transition and promotes tumor cell proliferation in non-small cell lung cancer. *Cancer Metab.* 2, 11 (2014).
11. Baer, S., Casaubon, L., Schwartz, M. R., Marcogliese, A. & Younes, M. Glut3 expression in biopsy specimens of laryngeal carcinoma is associated with poor survival. *Laryngoscope* 112, 393–396 (2002).
12. Tsai, T.-H. *et al.* Overexpression of GLUT3 promotes metastasis of triple-negative breast cancer by modulating the inflammatory tumor microenvironment. *J. Cell Physiol.* 236, 4669–4680 (2021).
13. Schlößer, H. A. *et al.* Glucose transporters 1, 3, 6, and 10 are expressed in gastric cancer and glucose transporter 3 is associated with UICC stage and survival. *Gastric Cancer* 20, 83–91 (2017).
14. Gao, H. *et al.* Prognostic value of glucose transporter 3 expression in hepatocellular carcinoma. *Oncol. Lett.* 19, 691–699 (2020).
15. Dai, W. et al. GLUT3 induced by AMPK/CREB1 axis is key for withstanding energy stress and augments the efficacy of current colorectal cancer therapies. Signal Transduct Target Ther. 5, 177 (2020).
16. Lodish H, Berk A, Zipursky SL, et al. Molecular Cell Biology. 4th edition. New York: W. H. Freeman; 2000.
17. Long W., Cheeseman C.I. Structure of, and functional insight into the GLUT family of membrane transporters. Cell Health Cytosk. 2015;7:167–183.
18. Uldry M., Thorens B. The SLC2 family of facilitative hexose and polyol transporters. Pflüg. Arch. 2004;447:480–489. doi: 10.1007/s00424-003-1085-0.
19. Zhao F.-Q., Keating A.F. Functional properties and genomic of glucose transporters. Curr. Genom. 2007;8:113–128. doi: 10.2174/138920207780368187.
20. Thorens B., Mueckler M. Glucose transporters in the 21st Century. AJP Endocrinol. Metab. 2010;298:E141–E145. doi: 10.1152/ajpendo.00712.2009.
21. Uldry M., Ibberson M., Horisberger J.-D., Rieder B.M., Thorens B. Identification of a mammalian H+-myo-inositol symporter expressed predominantly in the brain. EMBO J. 2001;20:4467–4477. doi: 10.1093/emboj/20.16.4467.
22. Quistgaard EM, Löw C, Guettou F, Nordlund P. Understanding transport by the major facilitator superfamily (MFS): structures pave the way. Nat Rev Mol Cell Biol. 2016;17(2):123-132. doi:10.1038/nrm.2015.25.
23. Jardetzky, O. Simple allosteric model for membrane pumps. *Nature* 211, 969–970 (1966).
24. Baker, G. F. & Widdas, W. F. The asymmetry of the facilitated transfer system for hexoses in human red cells and the simple kinetics of a two component model. *J. Physiol.* 231, 143–165 (1973).
25. Carruthers, A. & Helgerson, A. L. Inhibitions of sugar transport produced by ligands binding at opposite sides of the membrane. Evidence for simultaneous occupation of the carrier by maltose and cytochalasin B. *Biochemistry* 30, 3907–3915 (1991).
26. Deng, D. *et al.* Crystal structure of the human glucose transporter GLUT1. *Nature* 510, 121–125 (2014).
27. Deng, D. *et al.* Molecular basis of ligand recognition and transport by glucose transporters. *Nature* https:// doi. org/ 10. 1038/ nature14655 (2015).
28. Nomura, N. *et al.* Structure and mechanism of the mammalian fructose transporter GLUT5. *Nature* 526, 397–401 (2015).
29. Mishra, R. K. *et al.* In silico modeling-based identification of glucose transporter 4 (GLUT4)-selective inhibitors for cancer therapy. *J. Biol. Chem.* 290, 14441–14453 (2015).
30. Thompson *et al.* Discovery of a specific inhibitor of human GLUT5 by virtual screening and in vitro transport evaluation. *Sci. Rep.* 6, 24240 (2016).
31. Schmidl, S. *et al.* Identification of new GLUT2-selective inhibitors through in silico ligand screening and validation in eukaryotic expression systems. *Sci. Rep.* 11, 13751 (2021).
32. Irwin JJ, Shoichet BK. ZINC-a free database of commercially available compounds for virtual screening. *J Chem Inf Model*. 2005;45(1):177-182.
33. Grandhi et al. (2023). Solvent-guided quantitative structure-activity relationship (SG-QSAR): *In silico* SG-QSAR-based improvement of the human uridine phosphorylase-2 inhibitor binding affinity with potential applications in reducing the toxicity of chemotherapy. TCABSE-J, 1(5):20-25.
34. Aggunna, M., Grandhi, A.V.K.S. and Yedidi, R.S. (2023). Molecular dynamics simulations of cytotoxin-associated gene A coded protein from Helicobacter pylori to probe the flexibility of p53 binding pocket for inhibitor design. TCABSE-J, Vol. 1, Issue 6:9-14.
35. Cuozzo et al. (2022). SwissBioisostere 2021: updated structural, bioactivity and physicochemical data delivered by a reshaped web interface. *Nucl. Acids Res. 50*(D1), D1382–D1390.

Full figure legends:

Figure 1. Homology model of human GLUT3.

Figure 2. SAL3 and SAL18 structures and binding profiles. The 2-dimensional structures of SAL13 and SAL18 are shown in the top row. The bottom row shows the overall binding profiles of SAL13 and SAL18 shown as white color stick models in the binding pocket of the human GLUT3 (shown in green color). Both bind deep into GLUT3.

Figure 3. MD simulations of GLUT3 with SAL13 (left) and SAL18 (right). The overall C_α RMSD and RMSF of GLUT3 docked with SAL13 (left column) and SAL18 (right column) over 15 ns MD simulations are shown here. Both the RMSD and RMSF profiles of GLUT3 look different for SAL13 and SAL18 indicating that they are bound differently in GLUT3.

Figure 4. SAL13 (left) and SAL18 (right) binding profiles. Both compounds show persistent contacts with GLUT3 throughout the MD simulation. SAL18 has a better binding profile compared to SAL13 overall.